Equatorial ionospheric zonal drift by monitoring local GPS reference networks

Shengyue Ji,[1] Wu Chen,[1] Xiaoli Ding,[1] and Chunmei Zhao[2]

[1]   The propagation of electromagnetic waves through the turbulent ionosphere produces scintillations through diffraction, and understanding the physical nature of scintillations is important for engineers and technologists as well as for scientists. In recent years, the establishment of the Global Positioning System (GPS) provided a new technique that can be used to study ionospheric scintillations. The usual way of doing that is the deployment of GPS receivers closely spaced in east-west magnetic direction and then estimating the zonal drift velocities based on the signal power observations. One of the weaknesses of this method is that high-rate sampling such as 20 Hz is required for close-spaced stations and generally no such data are available for studying ionospheric scintillation in the past years. In this research work, a scintillation monitoring method based on slant TEC (STEC) observations of local GPS Continuously Operating Reference Station (CORS) network is proposed. First, the past research works on the equatorial ionospheric drift velocities are summarized. Then, by comparing the scintillation pattern of the signal power and STEC observations of California local GPS reference network, we find that the STEC is a good choice for estimating the ionospheric zonal drift velocity. Then it is illustrated how to calculate the ionospheric scintillation velocity based on STEC. Finally, the proposed method is applied to Hong Kong GPS reference network and several cases of the calculated ionospheric zonal velocities are given.

1.   Introduction

[2]   Ever since its peculiarities were first noticed sixty years ago, the equatorial ionosphere has been the venue of many ground-based and spaced-based experiments, the subject of much speculation, the topic of innumerable papers, and the source of much interesting physics.

[3]   Within a few degrees of the geomagnetic equator, the ionosphere has features that are not found elsewhere. The equatorial ionosphere undergoes dramatic changes following sunset as a result of the eastward electric field that is attributed to the F region dynamo [*Rishbeth*, 1971; *Heelis et al.*, 1974; *Farley et al.*, 1986; *Crain et al.*, 1993]. When released by the decrease of the solar E region conductivity following sunset, this field produces an upward E × B drift of the F layer plasma above the dip equator that give rise to three important phenomena that can dominate the ionosphere throughout a wide expanse of latitude and longitude for several hours.

[4]   The first and most major disturbance of these phenomena is the equatorial bubble which is a region of reduced density containing small scale irregularities. The bubble has been the subject of experimental and theoretical studies for many years [*Woodman and La Hoz*, 1976; *Tsunoda and White*, 1981; *Kelley*, 1989; *Mendillo et al.*, 1992]. A bubble typically forms following sunset, drifts eastward, and rises in altitude extending increasingly northward and southward along the geomagnetic field. Of particular importance is the fact that the ionospheric irregularities within the bubble cause scintillation that can seriously disrupt the operation of nearly all space and ground-based systems that rely on transionospheric propagation of radio frequencies [*Aarons*, 1993].

[5]   A second phenomenon is bottomside spread F (BSSF), irregularities that occur below the F layer maximum [*Woodman and La Hoz*, 1976; *Argo and Kelley*, 1986; *Flaherty et al.*, 1996; *Hysell and Burcham*, 1998]. In being limited to a thin layer in altitude, BSSF extends via the magnetic field to a narrow band in latitude [*Aarons*, 1993]. It typically forms continuously following sunset, and then drifts eastward. Though less disruptive than bubbles, BSSF produces increased VHF scintillation [*DasGupta et al.*, 1983] and interferes with HF propagation particularly during solar maximum.

[6]   A third phenomenon is the enhancement of the Appleton or equatorial anomaly, regions of high F layer electron density maximizing about 15° in latitude north and south of the dip equator that have been studied observa-

[1]Department of Land Surveying and Geo-Informatics, Hong Kong Polytechnic University, Hong Kong.
[2]Chinese Academy of Surveying and Mapping, Beijing, China.

tionally and theoretically for many years [*Anderson*, 1973; *Moffett*, 1979; *Abdu et al.*, 1990]. Following sunset, particularly during solar maximum, E × B drift and diffusion enhance the transport of plasma to the regions which contain the highest maximum electron densities and, when bubbles intersect them, produce the highest levels of scintillation effects observed worldwide [*Klobuchar et al.*, 1991]. The effect of the enhanced electron density is to create errors in the Global Positioning System and radar location and also to interfere with HF propagation.

[7] Scintillations occur when electromagnetic waves traverse a region of irregularities containing fluctuations in the index of refraction and can cause a signal's amplitude or phase to fluctuate about its mean level because the signal's electromagnetic energy is scattered and redistributed by the disturbed ionospheric F region. Before entering the region of irregularities the electromagnetic wave possesses a front of constant phase. After exiting the region of irregularities the previously constant phase front varies in phase, depending on the nature of the index of refraction irregularities.

[8] The occurrence of scintillations has been studied for several decades and its morphology has been documented extensively for the auroral, midlatitude and equatorial regions [*Aarons*, 1977, 1982]. The most intense scintillations have been observed in the nighttime equatorial region.

[9] The ionospheric irregularities causing the scintillations are constantly in motion, due to the presence of neutral air winds and electric and magnetic fields. The drift velocity of the irregularities can be estimated from the time lags of the scintillations observed with several receivers at spaced intervals [*Valladares et al.*, 1996; *Kil et al.*, 2000; *Kintner and Ledvina*, 2004]. Through spaced receiver and incoherent backscatter techniques, the equatorial irregularities have been found to drift in the magnetic east-west direction, with a vertical component of drift present as well [*Woodman*, 1970; *Paulson*, 1984]. The drift velocities just after local sunset may vary considerably from the postmidnight velocities.

[10] The study of ionospheric plasma drifts is of fundamental importance in understanding the F region dynamo and the equatorial spread F phenomenon in the low-latitude region. The plasma drifts perpendicular to the magnetic field as a result of the polarization electric fields generated by the neutral wind-driven currents in the ionosphere [*Heelis et al.*, 1974; *Richmond et al.*, 1976; *Farley et al.*, 1986]. During daytime the *E* region electric fields produced by the tidal winds control the plasma drift in the F region. After sunset, the E region conductivity is much reduced, and the plasma drifts eastward under the control of the F region dynamo electric fields.

[11] The extensive observations of the zonal drift velocity at the magnetic equator have been made with incoherent scatter radar [*Woodman*, 1972; *Fejer*, 1981; *Fejer et al.*, 1991], the DE-2 satellite measurements of the vertical electric field [*Aggson et al.*, 1987; *Coley and Heelis*, 1989; *Fejer et al.*, 1995] and from the movement of the airglow images [*Mendillo and Baumgardner*, 1982; *Abdu et al.*, 1987; *Rohrbaugh et al.*, 1989; *Sobral and Abdu*, 1990, 1991; *Tinsley et al.*, 1997; *Pimenta et al.*, 2003b; *Martinis et al.*, 2003].

[12] The establishment of Global Positioning System (GPS) has provided a new set of tools for the research of ionospheric irregularities and their effect on the radio wave propagation [*Aarons et al.*, 1996; *Kelley et al.*, 1996; *Beach et al.*, 1997; *Musman et al.*, 1997]. Compared to the other techniques, the advantage of GPS is a comparatively larger number of satellites, 6–12 compared to 1–2 for most geostationary experiments. The successful observations of the zonal drift velocity have been made with GPS in past research works and the general way of doing this is based on the observed signal power of two closely spaced GPS receivers in east-west direction [*Kil et al.*, 2000; *Kintner et al.*, 2001; *Kil et al.*, 2002; *Kintner and Ledvina*, 2004; *Makela et al.*, 2004; *Otsuka et al.*, 2006].

[13] Research works about scintillation have been done in many parts of world, especially in low-latitude areas, such as Ancon in Peru, Cochoeira Paulista in Brazil, Korhogo in Ivory Coast, and others, but few have been found in Hong Kong.

[14] Hong Kong is a low-latitude area with geographic coordinates around latitude: 22.33 N, longitude: 114.20 E (magnetic latitude around 14.5 N) and ionospheric scintillation can be observed frequently [*Chen et al.*, 2008]. The objective of this research is to provide a way of monitoring ionospheric scintillation based on local GPS network in Hong Kong area.

[15] In this paper, after a brief review of past research works and description of scintillation velocity estimation principle, the new estimating method with slant total electron content (STEC) data derived from GPS observations is introduced. Then this new method is first tested based on observations in California GPS network. This may seem a little strange as California is a midlatitude location and our research is dedicated to Hong Kong area. The reason of doing this is that in the past research works of scintillation velocity estimation with GPS, the observed signal power is usually used. But in the Hong Kong GPS network, no such observation is available. The GPS observations in California are the only data source we find, that has both signal power and carrier phase observations. After demonstrating that STEC observation is better choice than observed signal power for scintillation monitoring based on local GPS network, our new method to estimate the drift speed based on STEC will be applied to Hong Kong area. The results show the estimated drift velocities are consistent with other studies.

2. Review of Past Research Works

[16] Ionospheric drift velocities at the magnetic equator and the anomalies are controlled by tidal winds and dynamo electric fields. During the day the F region is driven westward through coupling to the E region and neutral winds. During the night the E region conductivity decreases, releasing the F region to drift eastward. This typical pattern has been established at the equator with incoherent scatter measurements [*Woodman*, 1972; *Fejer*, 1981; *Fejer et al.*, 1991], using satellite measurements of electric field [*Aggson et al.*, 1987; *Coley and Heelis*, 1989; *Fejer et al.*, 1995], observing the drift of total electron content depletions [*Abdu et al.*, 1985], following the movement of ionospheric structure in airglow the movement of ionospheric structure in airglow images [*Mendillo and Baumgardner*, 1982; *Abdu et al.*, 1987; *Rohrbaugh et al.*, 1989; *Sobral*

and Abdu, 1990, 1991; *Tinsley et al.*, 1997; *Pimenta et al.*, 2003b; *Martins et al.*, 2003], and by observing the drift of scintillation fade patterns from geostationary satellite signals [*Abdu et al.*, 1985, 1987; *Basu et al.*, 1996; *Valladares et al.*, 1996].

[17] The most extensive observations of the zonal drift velocity at the magnetic equator have been made from incoherent scatter radar station at Jicamarca in Peru [*Woodman*, 1972; *Fejer*, 1981]. The drift pattern shows a typical diurnal cycle consisting of westward drifts with 50 m/s during the day and eastward drifts up to 130 m/s in the evening. A gradual decrease is observed in the zonal drift velocity from between 100 and 200 m/s at around 22:00 LT to below 50 m/s after local midnight [*Mendillo and Baumgardner*, 1982; *Mendillo et al.*, 1997; *Taylor et al.*, 1997; *Sinha and Raizada*, 2000; *Pimenta et al.*, 2003b]. However, other researchers have seen a slight increase in the drift velocity near local midnight [*Tinsley et al.*, 1997; *Santana et al.*, 2001; *de Paula et al.*, 2002; *Makela and Kelley*, 2003; *Mukherjee*, 2003]. Still others have at times seen zonal drift velocities as fast as 400 m/s [*Fagundes et al.*, 1997]. The differences seen in some of the studies simply highlight the fact that significant variability in drifts occur day to day, and between different seasons, latitudes, and longitudes.

[18] The ionospheric irregularities present a large dependence on the solar cycle, the local time, the season, the location and the magnetic disturbances etc. The ionospheric irregularities have very large day-to-day variability during quiet and disturbed times, which is due to the various factors affecting the generation and growth of plasma interchange instabilities, and is still an enigmatic problem [*Abdu et al.*, 2002]. The most well recognized influences on irregularity growth are the height and vertical drift of the F layer driven by the eastward electric field.

[19] The typical pattern of equatorial F region ionospheric drifts has been established. However, there exist departures from this typical pattern especially during periods of magnetic storms, for example, brief periods of westward drift at night [*Basu et al.*, 1996; *de Paula et al.*, 2004; *Kintner and Ledvina*, 2004].

[20] During geomagnetic storms, the magnetospheric electric field can, under favorable conditions, penetrate directly to low latitudes almost instantaneously, and also, with a delay of 9–30 h, through the disturbance dynamo mechanism [*Kikuchi and Araki*, 1979; *Blanc and Richmond*, 1980; *Fejer*, 1986; *Spiro et al.*, 1988; *Fejer et al.*, 1990; *Fejer and Scherliess*, 1995; *Scherliess and Fejer*, 1997]. The disturbance dynamo electric field reduces the plasma ascent rate at equatorial latitudes during daylight but also reduces the descent rate at night, decreasing the threshold for inversion. Direct penetration can be eastward, lifting the equatorial plasma, or westward, lowering the plasma. At night, eastward direct electric field penetration could trigger ionospheric irregularities at any time of year since it lifts the plasma and creates favorable conditions for irregularities to grow. This effect can be intensified if the eastward direct penetration occurs in conjunction with the regular post-sunset prereversal enhancement driven by *F* region dynamo action [*Batista et al.*, 1991] or with disturbance dynamo action at night.

[21] A few studies have begun to address the latitudinal variation of the zonal drift velocity. One study found that two peaks in the zonal drift velocity were seen [*Pimenta et al.*, 2003a]. The first was located at about 19°S between 20:00 and 22:00 LT, while the second occurred a bit later at the magnetic equator between 21:00 and 22:00 LT. They also found a valley in the zonal drift velocity at approximately 10°S. Another study found that in the postsunset period, the eastward plasma drifts at the magnetic equator are smaller than near the anomaly region [*Martinis et al.*, 2003]. However, this relationship reverses near 23:00 LT.

[22] Table 1 gives a summary of equatorial ionospheric zonal drift velocity of past research works. From Table 1, we can see that generally the velocity is between 100 and 200 m/s after sunset and before midnight, and the drifting direction is eastward. The bold results in Table 1 show the typical pattern of equatorial F region ionospheric drifts; that is, the eastward drifting velocity decreases gradually after sunset, then turns to west steadily after midnight.

[23] The italic part in Table 1 shows some of the research results that do not agree with the above typical pattern. The equatorial ionospheric zonal drifting direction can be westward after sunset or the drifting direction after midnight does not turn west, it is still in east direction and the velocity can increase again.

[24] The underline part in Table 1 shows the large day-to-day variability and the difference can be almost 100 m/s for the same time of two neighboring days.

3. Zonal Drift Velocity Estimation With Cross-Correlation Method

3.1. Measuring the Velocity of a Diffraction Pattern

[25] A diffraction pattern in signal power moving across the ground has a measurable velocity. Assume that the pattern is slowly changing and traverses zonally. The optimal time delay between the receivers of the traversing diffraction pattern can be calculated using the cross-correlation technique [*Mitra*, 1949; *Briggs*, 1968]. The cross-correlation function between two signals with signal power time series, S_1 and S_2 is:

$$C(T) = \frac{\sum_k S_1(t_k) S_2(t_k - T)}{\sqrt{\sum_k S_1^2(t_k) \sum_k S_2^2(t_k - T)}} \qquad (1)$$

where *T* is the lag and k is an index into the signal time series. The value of *T* that maximizes $C(T)$ is the optimal lag $-T_0$.

[26] In order to calculate the apparent velocity of the diffraction pattern, the distance that the irregularity layers move in the ionosphere is required. In the past research works, the horizontal distance between two zonally aligned and close-spaced GPS receivers is generally used with a correction of 4% and only observations made at high elevations (>40°) are included [*Kil et al.*, 2002]. The distance that the irregularity layers move in the ionosphere is actually the distance between two Ionospheric Pierce Points (IPP) (Ionospheric Pierce Point is the intersection point of the line from a receiver to a satellite with the ionospheric layer of F peak) from the two receivers. In this study, the distance will be calculated using two IPP points from two GPS receivers and the altitude from the receiver to the F peak is assumed to be 350 km.

Table 1. Summary of Equatorial Ionospheric Zonal Drift Velocity of Past Research Works

Place	Latitude and Longitude	Instrument	Date	Direction	Velocity	Hour	Reference
Ancon, Peru	**11.8S 77.2W**	**Geostationary satellite**	**1/3/1999** **22/10/1999**	**first eastward** **then westward**	**200 – (−50)** **200 – (−300)**	**21:00–24:30–29:00** **19:00–24:00–31:00**	*Bhattacharyya et al.* [2002]
Cachoeira Paulista	*22.7S 45.0W*	*OI 630 nm*	*24/2/1995*	*eastward*	*300* *250* *300* *210*	*22:20–23:00* *23:20–23:40* *24:00* *00:20–00:40*	*Fagundes et al.* [1997]
Cachoeira Paulista	22.7S 45.0W	OI 630 nm	25/2/1995	eastward	400 100 200	21:20–21:40 21:40–22:00 22:00–22:40	*de Paula et al.* [2002]
Cachoeira Paulista	22.7S 45.0W	GPS	8/11/1998	eastward	0–200	After 20:30	
Cachoeira Paulista	22.7S 45.0W	GPS	12/1998 1–2/1999	eastward	180–50	21:00–25:00	*de Paula et al.*, 2002
Cachoeira Paulista	**22.7S 45.0W**	**OI 630 nm**	**26/8/1998**	**first eastward,** **then westward**	**30** **0** **−30** **−70**	**21:00** **22:30** **24:00** **27:30**	*Abdu et al.* [2003]
Korhogo, Ivory Coast	9.4N 5.61W	Multifrequency HF radar	24/10/1994 27/5/1993	westward	120 (110 km height) 150(142 km) 170(180 km) 180(215 km) 190(236 km) 300(275 km)	daytime	*Farges and Blanc* [2002]
Kwajalein atoll	8.737N 167.738E	NASA sounding rocket with Altair VHF/UHF scatter radar	8/2004	eastward westward	190 m/s above 250 km 50 m/s below 250 km	20:52:56	*Hysell et al.* [2005]
Kototabang, Indonesia	0.2S 100.32E	GPS	3–4/2003–2004 9–10/2003–2004	eastward	150–50	20:00–25:00	*Otsuka et al.* [2006]
Kolhapur	16.8N 74.2E	OI 630 nm	25/3/1998	eastward	124 121 55 25	21:00 22:00 23:00 24:00	*Hari Kishore and Mukherjee* [2007]
Kolhapur	16.8N 74.2E	OI 630 nm	14/3/1999	eastward	134 122 110 112 76	21:00 22:00 23:00 24:00 25:00	
Kolhapur	16.8N 74.2E	OI 630 nm	14/4/1999	eastward	163 125 105 103	21:00 22:00 23:00 24:00	
Kolhapur	16.8N 74.2E	OI 630 nm	1/3/2000	eastward	197 192 190 126 82	21:00 22:00 23:00 24:00 25:00	
Kolhapur	16.8N 74.2E	OI 630 nm	2/3/2000	eastward	251 148	22:00 23:00	

Table 1. (continued)

Place	Latitude and Longitude	Instrument	Date	Direction	Velocity	Hour	Reference
Kolhapur	16.8N 74.2E	OI 630 nm	3/3/2000	eastward	67	24:00	Banola et al. [2005]
					41	26:00	
					228	22:00	
					208	23:00	
					163	24:00	
					130	25:00	
					120	26:00	
Kolhapur	16.8N 74.2E	OI 630 nm	5/3/2000	eastward	207	21:00	
					180	22:00	
					144	23:00	
Kolhapur	16.8N 74.2E	OI 630 nm	26/3/2001	eastward	262	21:00	
					112	22:00	
					115	23:00	
					150	24:00	
Mumbai	19N 73E	Geostationary satellite	14/12/1994	eastward	101.8	21:46	
			2/12/1995		71.3	21:53	
			30/1/1995		40.7	23.27	
Naval Communication Area Master Station	12.4N 147.0E	UHF channel Geostationary satellite	6/5/1982	eastward	175–90	21:00–25:00	Spatz et al. [1988]
			30/1/1983		130–50	22:00–25:00	
On equator	geomagnetic longitude 160–240 50–130	Spectrographic Imager-13	1/5/2002	eastward	Average 165 66–333 Peak:500	5–11 UT 14–20 UT	Immel et al. [2004]
Panhala	*17N 74.2E*	*OI 630 nm*	*22/1/2001*	*eastward*	*206*	*21:00*	Hari Kishore and Mukherjee [2007]
					137	*22:00*	
					85	*23:00*	
					109	*24:00*	
					170	*25:00*	
Panhala	17N 74.2E	OI 630 nm	25/1/2001	eastward	262	21:00	
					197	22:00	
					146	23:00	
					163	24:00	
					119	25:00	
Panhala	17N 74.2E	OI 630 nm	18/2/2001	eastward	132	21:00	Banola et al. [2005]
					162	22:00	
					169	23:00	
					110	01:00	
Panhala	17N 74.2E	OI 630 nm	19/2/2001	eastward	201	21:00	
					147	22:00	
					139	23:00	
					80	24:00	
Pondicherry	12N 79.1E		14/12/1994	eastward	98.9	21:06	
			2/12/1995		79.2	21:39	
			30/1/1995		89.1	23.08	
São José dos Campos	23.21S 45.86W	OI 630.0 nm OI 777.4 nm	23/10/2000	eastward	150–20	20:00–25:30	Abalde et al. [2004]
			30/10/2000		150	22:00	
			21/2/2001		180–50	21:00–24:00	
			15/10/2001		200–100	21:00–25:00	

Table 1. (continued)

Place	Latitude and Longitude	Date	Instrument	Direction	Velocity	Hour	Reference
São Luís, Brazil	2.33S 315.8E	18/12/2001	GPS	eastward	180–110	22:00–25:00	de Paula et al. [2004]
São Luís, Brazil	2.33S 315.8E	2/3/2002	GPS	eastward	100, 90	22:00, 24:30	de Paula et al. [2004]
São Luís, Brazil	2.33S 315.8E	8/3/2002	GPS	eastward	145, 120, 160, 140	20:30	de Paula et al. [2004]
São Luís, Brazil	*2.33S 315.8E*	*11/4/2001*	*GPS and Radar*	*westward*	*(−250)–(−100)*	*18:50–19:20*	*de Paula et al. [2004]*
Sata, Japan	31N 130.7E	12/11/2001	630 nm all sky imager	eastward	100	23:57–01:27	Otsuka et al. [2002]
Darwin, Australia	12.4S 131.0E	12/11/2001	630 nm all sky imager	eastward	100	23:57–01:27	Otsuka et al. [2002]
Tirunelveli	8.7N 77.7E	14/12/1994, 2/12/1995	Radio beacon form geostationary satellite FLEETSAT or INMARSAT	eastward	118.5, 69.1	20:34, 21:30	Banola et al. [2005]
Waltair	17.7N 83.3E	22/7/2004	geostationary satellite	eastward	250–100	18:30–26:00	Rama Rao et al. [2005]
Waltair	17.7N 83.3E	27/5/2004	geostationary satellite	westward	65, 0.57	03:06–03:08	Rama Rao et al. [2005]
Wuhan	*30.53N 114.36E*	*10/11/2004*	*GPS*	*westward*	*120–40*	*14:00–18:00*	*Xu et al. [2007]*

[27] Assuming the distance between two IPPs is d, the apparent velocity of the diffraction pattern is then d/T_0.

[28] Using a method of modeling correlated diffraction patterns as concentric ellipses, the true velocity is defined as:

$$v = \frac{\acute{v}}{1 + t_0^2/T_0^2} \qquad (2)$$

where t_0 is the time at which the autocorrelation function equals the peak of the cross correlation function $\acute{v}$ and is the apparent velocity.

[29] The error assuming that the apparent velocity is equal to the true velocity is 6% for the worst case and 1% typically [*Kintner and Ledvina*, 2005]. In this paper, apparent velocity instead of true velocity will be estimated and used.

3.2. Relationship Between Diffraction Pattern Velocity and Ionospheric Drift Velocity

[30] The diffraction pattern velocity is defined in the horizontal plane, i.e., the plane occupied by the receivers. The diffraction pattern velocity is a function of the ionospheric drift velocity, mean scattering height, and satellite velocity. Mathematically, the diffraction pattern velocity is [*Costa and Fougere*, 1988]:

$$v_{diff} = \frac{h_s}{h_s - h_{ion}}\left\{ v_{ion-z} \right.$$
$$\left. - \tan(\theta)k_h v_{ion-v} - \frac{h_{ion}}{h_s}[v_{s-z} - \tan(\theta)k_h v_{s-v}] \right\} \qquad (3)$$

where v_{diff} is the zonal diffraction pattern velocity in the receiver plane, h_s is the height of the satellite above the receiver plane, h_{ion} is the height of the scattering region, v_{ion-z} is the zonal ionospheric velocity in the horizontal plane, v_{ion-v} is the ionospheric velocity in the vertical direction, θ is the zenith angle of the vector from the receiver to the satellite, k_h is the unit vector projection in the horizontal plane of the vector from the receiver to the satellite, and v_{s-z} is the zonal satellite velocity in the plane defined by $h = h_s$, and v_{s-v} is the satellite velocity in the vertical direction.

[31] Note that equation (3) is subject to the assumption that the distributions of irregularities along the raypath that cause the signal to scintillate must occupy a significantly thin layer.

[32] Equation (3) has three unknowns: the mean scattering height, irregularity zonal velocity, and the irregularity vertical velocity. It cannot be solved analytically at a single instant in time. The simple straightforward way to determine ionospheric zonal drift velocity is to use the measured diffraction pattern velocity along with an assumed scattering height and vertical velocity.

[33] Generally the vertical velocity is assumed to be zero and a typical assumption for the mean scattering height is 350 km, corresponding to the typical F peak height. Then the estimate of the zonal ionospheric velocity is given by:
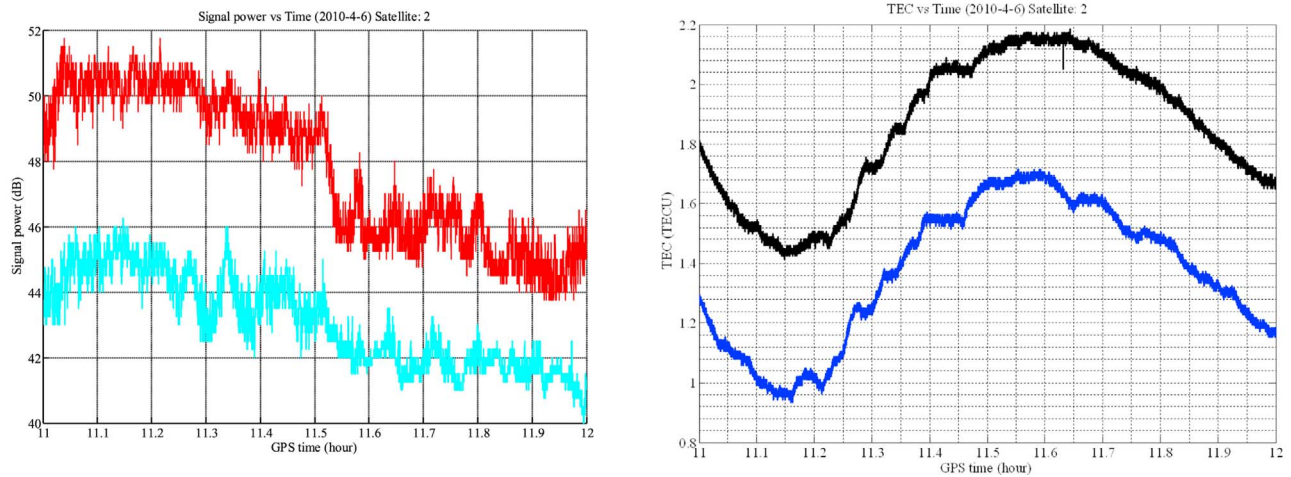
$$v_{ion-z} = \frac{h_s - h_{ion}}{h_s}v_{diff} + \frac{h_{ion}}{h_s}[v_{s-z} - \tan(\theta)k_h v_{s-v}] \qquad (4)$$
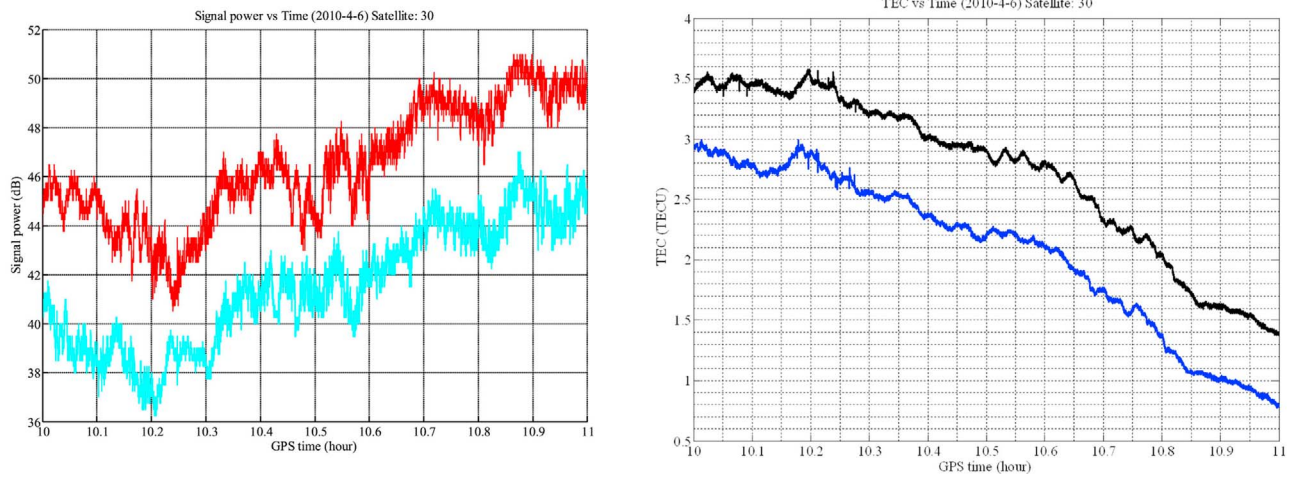
Figure 1. Observed (left) signal power and (right) STEC of satellite PRN 30 at 10:00–11:00 UT (GPS time) on 6 April 2010.
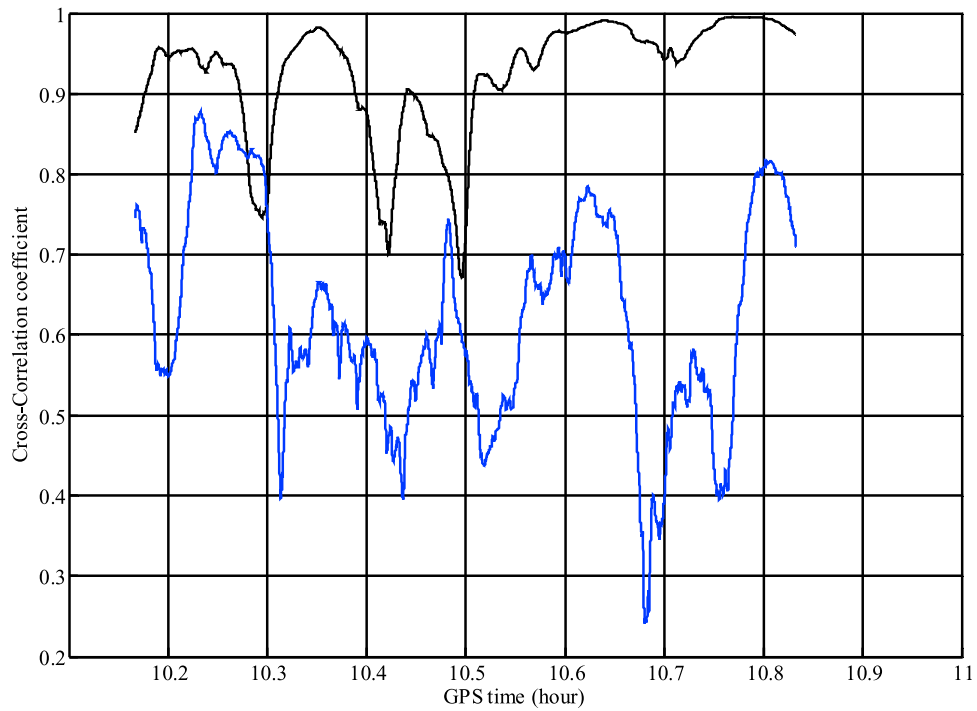
Figure 2. Cross-correlation coefficients (black, STEC; blue, signal power) of satellite PRN 30 at 10:00–11:00 UT (GPS time) on 6 April 2010.

Figure 3. Observed (left) signal power and (right) STEC of satellite PRN 2 at 11:00–12:00 UT (GPS time) on 6 April 2010.

The estimate given by equation (4) is not exact. However, past research works have shown that this method is applicable [*Beach and Kintner*, 1999; *Kil et al.*, 2000].

4. Slant Total Electron Content

[34] To achieve 3D tomography of the ionospheric electron distribution, it is necessary to get line-of-sight TEC from ground-based dual-frequency GPS measurements first. The basic observation equations of GPS phase and code

measurements of frequency from receiver to satellite can be expressed as follows:

$$\varnothing_{kj}^i = R_j^i - \alpha_k I_j^i - \lambda_k \left(b_{kj}^i + N_{kj}^i \right) \qquad (5)$$

$$P_{kj}^i = \left(R_j^i - \alpha_k I_j^i + dq_{kj} + dq_k^i \right) \qquad (6)$$

where $\alpha_k = 40.3/f_k^2$; λ_k is the wavelength; R_j^i is the sum of true distance; troposphere delay and clock bias correction; I_j^i
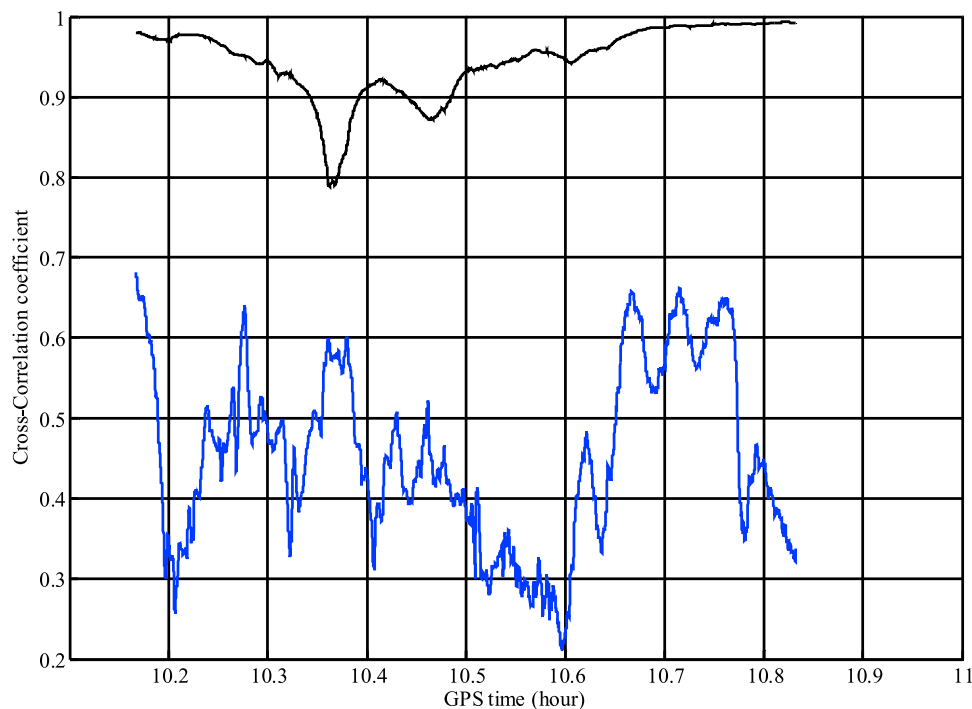
Figure 4. Cross-correlation coefficients (black, STEC; blue, signal power) of satellite PRN 2 at 11:00–12:00 UT (GPS Time) on 6 April 2010.
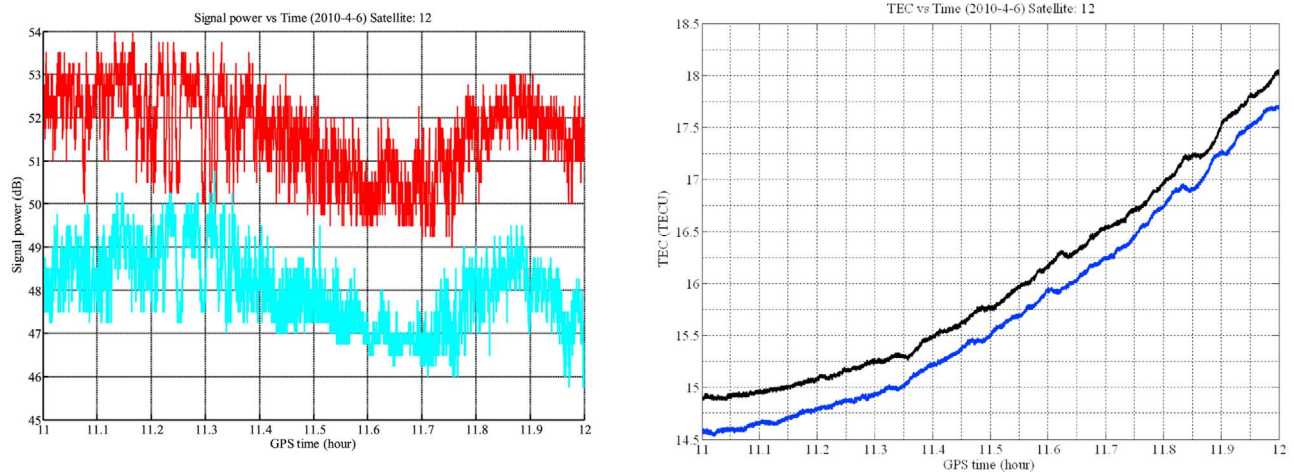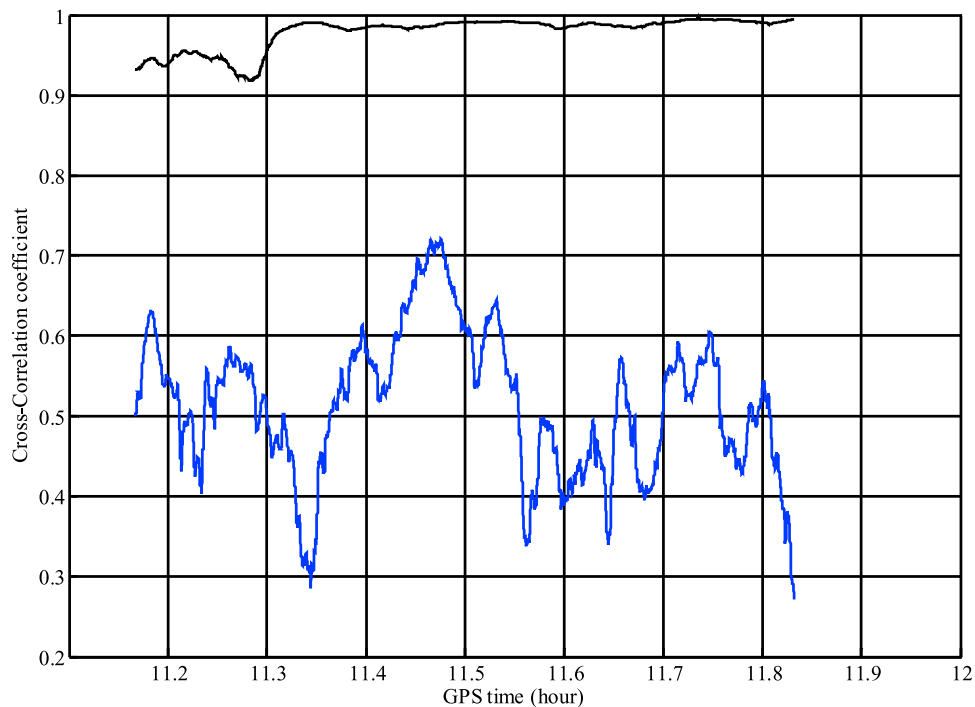
Figure 5. Observed (left) signal power and (right) STEC of satellite PRN 12 at 11:00–12:00 UT (GPS time) on 6 April 2010.

is the ionospheric delay; b_{kj}^i is the phase delay of satellite and receiver instrument bias; N_{kj}^i is the integer ambiguity; dq_{kj} and dq_k^i are the group delay of satellite and receiver instrument bias respectively. From equations (5) and (6), the following equation can be derived:

$$L_4 = \varnothing_{1j}^i - \varnothing_{2j}^i = -40.3 \left(\frac{1}{f_1^2} - \frac{1}{f_2^2} \right) STEC + B_4 \qquad (7)$$

$$P_4 = P_{1j}^i - P_{2j}^i = 40.3 \left(\frac{1}{f_1^2} - \frac{1}{f_2^2} \right) STEC + b_4 \qquad (8)$$

where STEC is the slant total electron content of GPS signal raypath; $B_4 = -\lambda_1(b_{1j}^i + N_{1j}^i) + \lambda_2(b_{2j}^i + N_{2j}^i)$; and $b_4 = (dq_{1j} - dq_{2j}) + (dq_1^i - dq_2^i)$. After the removal of cycle slips and outliers in the original carrier phase and pseudorange measurements, b_4 can be estimated based on SLM model and B_4 can be obtained through the formula $\sum_{i=1}^n (P_4 + L_4 - b_4)/n$

Figure 6. Cross-correlation coefficients (black, STEC; blue, signal power) of satellite PRN 12 at 11:00–12:00 UT (GPS time) on 6 April 2010.
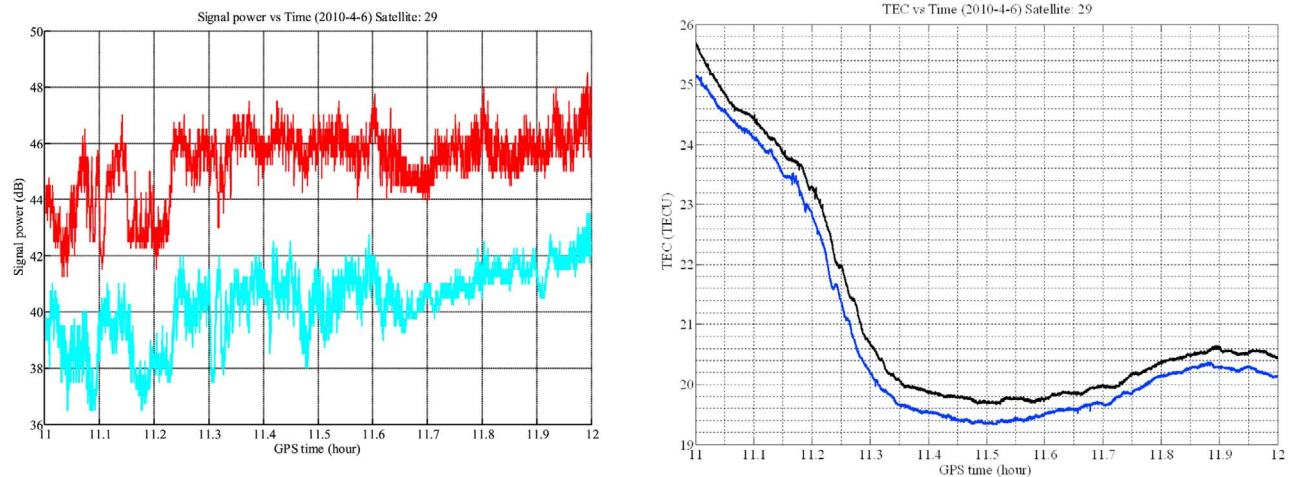
Figure 7. Observed (left) signal power and (right) STEC of satellite PRN 29 at 11:00–12:00 UT (GPS time) on 6 April 2010.

(n is the number of epochs). After that, STEC can be obtained from equations (7) or (8).

## 5. Zonal Drift Velocity Estimation Based on the GPS Reference Network in California

[35] The GPS reference network in California is composed of many stations and the data can be downloaded from ftp://garner.ucsd.edu/. On 6 April 2010, observations with sample interval of 0.2 s are provided. Two stations with

the names P494 and P496 are selected for the velocity estimation. Their geographic latitude and longitude are P494 (32°45′35″N, 115°43′55″W) and P496 (32°45′02″N, 115° 35′45″W) and their magnetic latitudes are around 39°29′24″N. We can see that, the baseline formed with these two stations is basically in east-west direction with a distance of 14 km.

[36] To estimate the ionospheric zonal drift velocity with these two stations, it is required that the ionospheric irregularities must be able to travel from one station to the other station and during the period the shape of the ionospheric
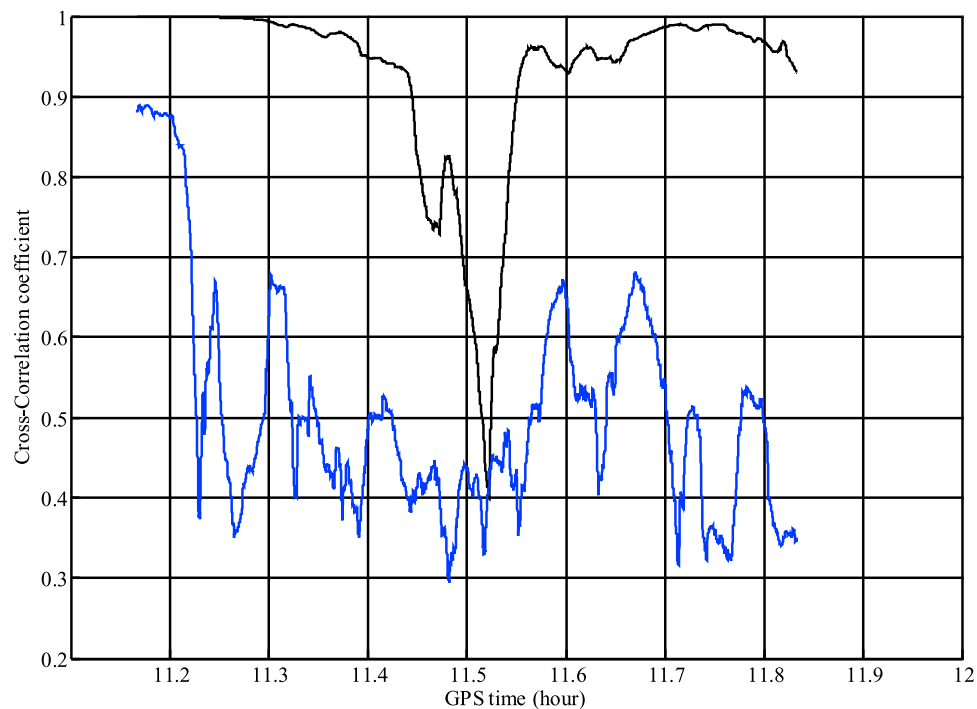
Figure 8. Cross-correlation coefficients (black, STEC; blue, signal power) of satellite PRN 29 at 11:00–12:00 UT (GPS time) on 6 April 2010.
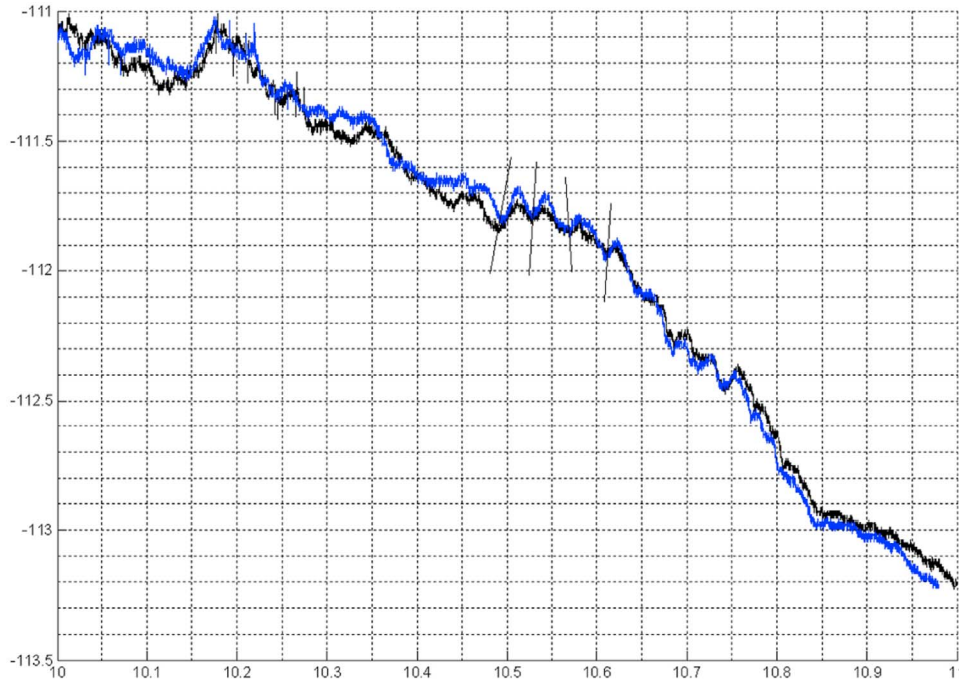
Figure 9. Rough matching of the STEC observations showed in Figure 1.

irregularities must have little change in order that the observations on these two stations are correlated to some degree. We find observations of a few satellites which look well correlated.

[37] Figures 1, 3, 5, and 7 show the observed signal power observations on frequency L1 (left) (note that for the convenience of comparison, the signal power observations on P494 (cyan line) are subtracted by 5, otherwise the two lines will be mixed together) and the slant TEC observations (right) of GPS satellite PRN 30 (GPS time: 10:00–11:00 UT; local time: 02:00–03:00 LT) and PRN 2, 12 and 29 30 (GPS time: 11:00–12:00 UT; local time: 03:00–04:00 LT) on the two stations on 6 April 2010. Obvious scintillation can be seen from Figures 1, 3, 5, and 7 (right). To get a good estimation of the zonal drift velocity, the observations on these two stations have to show similar scintillation pattern. In order to check which type of observation has more similar scintillation pattern, the cross-correlation coefficients are calculated for both of them according to the following steps: (1) calculate the mean value for each time series observation; (2) calculate the cross-correlation coefficient with maxi-

mum absolute value at observation time t_k for all possible lag time T,

$$\text{Max}(C(T)) = \text{Max}$$

$$\cdot \left(abs \left(\frac{\sum_{t_k-\frac{\tau}{2}}^{t_k+\frac{\tau}{2}}(S_1(t_k) - M_1)(S_2(t_k - T) - M_2)}{\sqrt{\sum_{t_k-\frac{\tau}{2}}^{t_k+\frac{\tau}{2}}(S_1(t_k) - M_1)^2 \sum_{t_k-\frac{\tau}{2}}^{t_k+\frac{\tau}{2}}(S_2(t_k - T) - M_2)^2}} \right) \right),$$

(9)

where M_1 and M_2 are the mean values of time series S_1 and S_2 of one type of observation and τ is the selected time span (5 min in this research work); and (3) all cross-correlation coefficients of each type of observation (signal power or STEC) will form a time series.

[38] Figures 2, 4, 6, and 8 give the cross-correlated coefficients from the observations of Figures 1, 3, 5, and 7. It is obvious that two STEC time series observations of the stations P494 and P496 are more correlated. This may be contributed by two reasons. The first reason is that the relative noise level of the signal power is much larger than

Table 2. Sampled Ionospheric Drift Velocities on 6 April 2010

Time	Elevation angle (deg)	Azimuth (deg)	IPP Position	Direction	Velocity From STEC (m/s)	Velocity From Signal Power (m/s)
02:30:00 LT	31.3	316.7	36.040107S, 119.607136W	westward	51	42
03:15:00 LT	25.5	296.7	35.150977S, 121.769085W	westward	258	133
03:18:00 LT	61.6	31.8	34.112458S, 114.719205W	westward	184	156
03:25:00 LT	81.9	223.8	32.437992S, 115.948914W	westward	213	138
03:37:00 LT	77.3	200.6	32.109556S, 115.878504W	westward	178	512
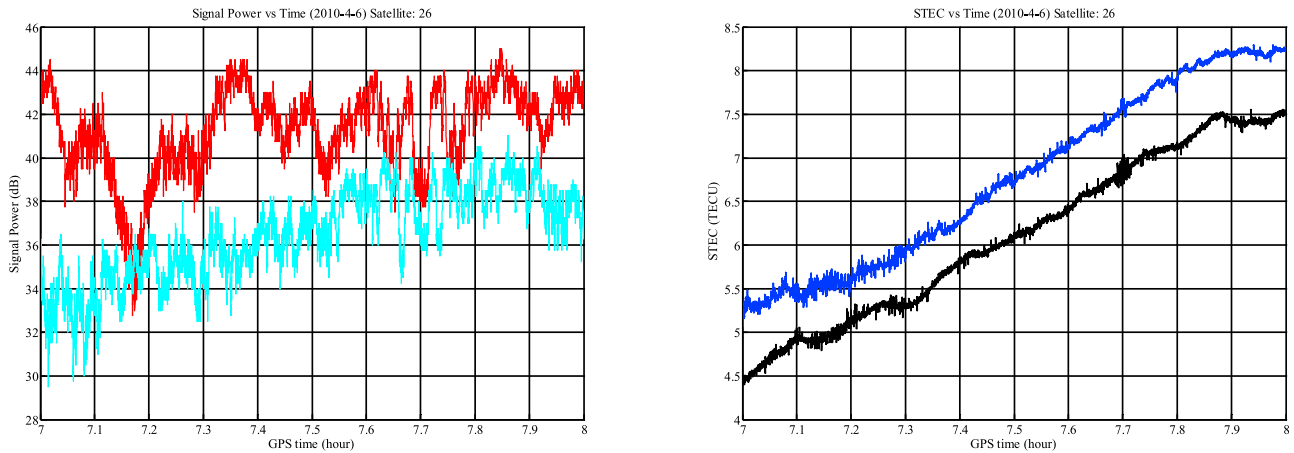
Figure 10. Observed (left) signal power and (right) STEC of satellite PRN 26 at 07:00–08:00 UT (GPS time) on 6 April 2010.

STEC. The second reason is that STEC is less sensitive to slight changes of ionosphere irregularities, as it is the integration of total electron content. This indicates that, the scintillation pattern of STEC observations is more similar than that of signal power observation and it is a better choice for estimating zonal drift velocity.

[39] In order to get the ionospheric zonal drift velocity from the STEC observations listed in Figures 1, 3, 5 and 7, the following steps are taken:

[40] First, roughly match the two wave-like lines of the STEC observations on the two stations by shifting one of them left or right. Figure 9 is an example after rough matching of the STEC observations showed in Figure 1.

[41] Second, identify all matching V- or Λ-like parts of the two wave-like lines. For example, in Figure 9, four almost vertical lines indicate four of them.

[42] Third, process each identified matching V- or Λ-like parts by cross correlation and get the time lag T_0 corresponding to the maximum cross-correlation coefficients based on equation (9).

[43] Fourth, get the distance D of the stations P494 and P496 in geomagnetic longitude direction and the apparent diffraction pattern velocity will be $v = D/T_0$.

[44] Finally, calculate ionospheric drift velocity according to equation (3). Table 2 lists the calculated ionospheric drift velocities at some sampled moments.

[45] The estimated velocities are a little higher compared to previous research works with a general value around 100–200 m/s. The drift direction after midnight is westward, which is consistent with the previous research works.

[46] For comparison, the drift velocities are also estimated using the received GPS signal powers from the two stations (also listed in Table 2). Except one case (last row in Table 2), the estimated velocities from the signal powers are generally less than the velocity derived from STEC, but with the similar magnitudes (50–150 m/s). For one case, the velocity estimated from the signal power is significantly larger than that from STEC, reaching over 500 m/s.
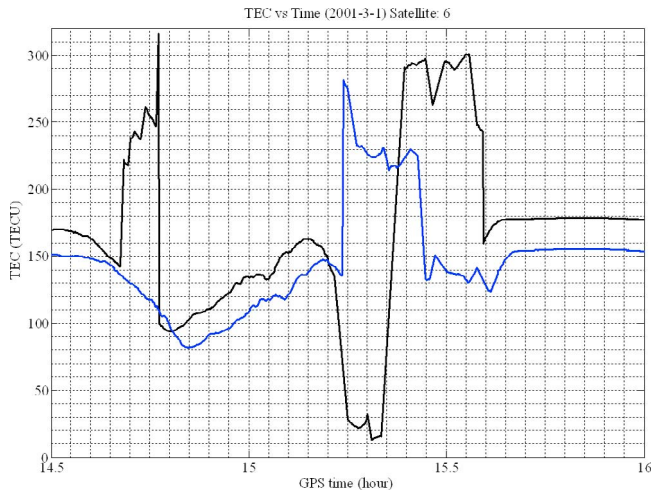
[47] However, most of the observations on these two stations are not correlated obviously. Figure 10 is one
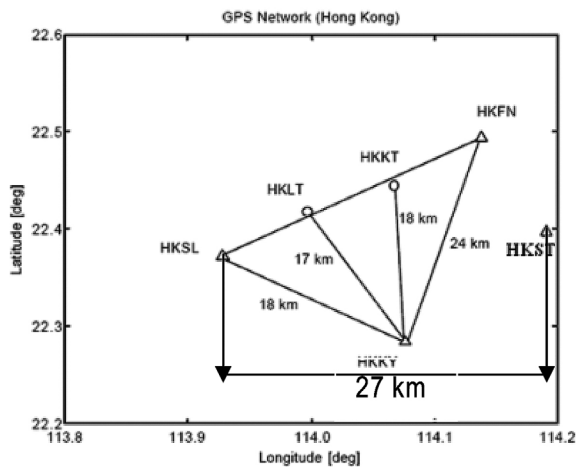
Figure 11. Hong Kong GPS active network stations.
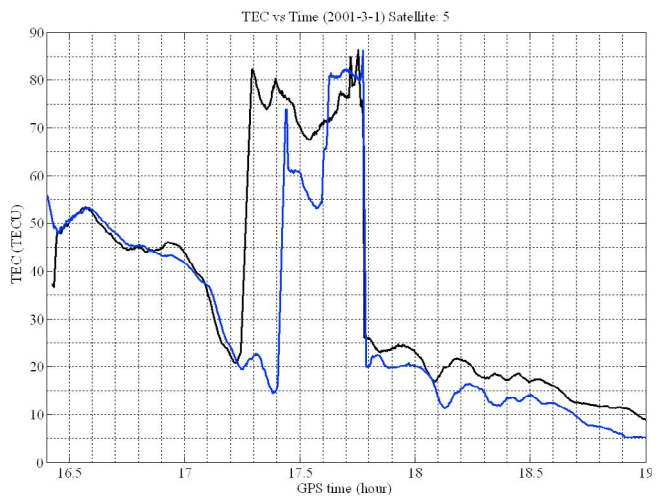
Figure 12. Observed STEC of satellite PRN 5 on 1 March 2001.

Figure 13. Observed STEC of satellite PRN 6 on 1 March 2001.

example of the observed signal power observations on frequency L1 (left) and the slant TEC observations (right) of GPS satellite PRN 26 on the two stations from GPS time 07:00–08:00 UT on 6 April 2010 (11:00–12:00 LT of local time). In Figure 10, we can see that, both the signal power observations and the STEC observations on station P496 (red and black lines) obviously have different scintillation from those of P494 (cyan and blue lines). This is probably due to the fact that the ionospheric scintillation is a local phenomenon: the ionospheric irregularities may not be able to travel that far or the shape changes a lot during the journey in this latitude (32°45′35″N) area.

6. Zonal Drift Velocity Estimation Based on the GPS Reference Network in Hong Kong

[48] In Hong Kong, there is a local GPS reference network, known as Hong Kong Satellite Positioning Reference Station Network (SatRef). It is developed and maintained by Survey and Mapping Office (SMO) of Lands Department of Hong Kong Government. From 2001 to 2003, during the 11 year solar cycle peak time, there were six GPS active network stations available as shown in Figure 11 (their magnetic latitudes are around 14°31′59″N). The distribution of GPS stations ranged from 22.2 to 22.5 degree in latitude and from 113.9 to 114.2 degree in longitude. Now the network consists of 12 Continuously Operating Reference Station (CORS) evenly distributed in Hong Kong. In its RINEX data, signal power observation is not recorded, so only STEC can be obtained.

[49] The stations used to investigate the scintillation propagation velocity are HKSL and HKST as they are basically in west-east direction and the sampled observations are recorded on 1–2 March 2001. The distance in east-west direction between the two stations is 27 km. The average hourly Dst indices for these two days are −4 and 0.6, and the average hourly Kp indices are 0.5 and 0.7. It shows that there were no magnetic perturbations of the Earth's atmosphere on these two days.

[50] On 1–2 March 2001 the observed STEC of satellite PRN 5, 6, and 9 on these two stations reflected the drift of the scintillation phenomenon as illustrated in Figures 12, 13, and 14. The line in black is the STEC on station HKSL and the line in blue is the STEC on station HKST. Figures 12, 13, and 14 clearly show that the scintillation patterns on these two stations are very similar and the time delay is obvious.

[51] Based on the distance in geomagnetic east-west direction between these two stations and the time delay and the procedures mentioned in the above section, the ionospheric drift velocities are estimated and listed in Table 3. Figure 15 is a map of the IPPs, which are the horizontal positions in ionospheric layer of altitude 350 km when scintillation happening and the estimated drift velocities are indicated by arrows (the length represents the velocity value and the pointing of the arrow represent the velocity direction).

[52] In Table 3, from the estimated drift velocity traced by satellites of both PRN 9 and 5, the gradual decrease with time is clear. However, though the time of the observed scintillation traced by satellite PRN 5 is later than that of PRN 9, its estimated velocity is much bigger than that of satellite PRN 9. We can get the reason from Figure 15, as it is noteworthy that the lower latitude, the faster the scintillation drifts except PRN 6 (but its scintillation position is far away from that of PRN 9 and 5 and the time is before midnight). This demonstrates that the velocity is not only related to time, but also related to the scintillation location (the IPP position).

[53] It is also noteworthy that the estimated drift velocities in Table 3 are still in eastern direction after midnight, but its value is gradually decreasing over time.

7. Conclusions

[54] In this research work, we are trying to monitor the equatorial ionospheric scintillation with STEC observations from a local GPS network and the detailed procedure is described. Two different areas are tested: one in California,
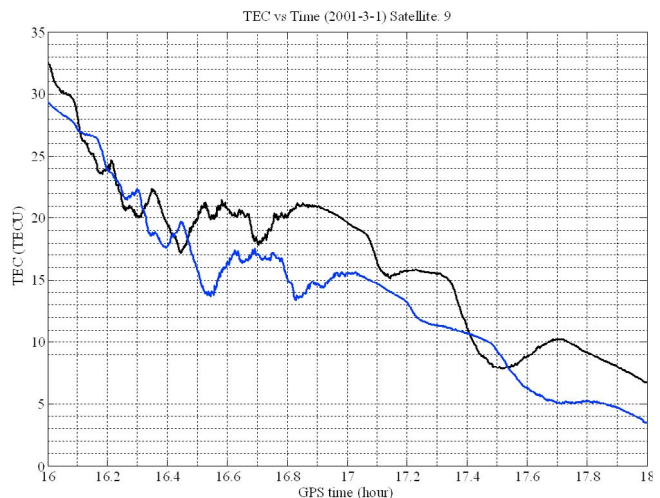
Figure 14. Observed STEC of satellite PRN 9 on 1 March 2001.

Table 3. Estimated Ionospheric Drift Velocities on 1–2 March 2001

PRN	Date	Local Time	Elevation Angle (deg)	Azimuth (deg)	IPP Position	Direction	Velocity (m/s)
6	1 Mar 2001	23:05:00	40.8	34.1	32.109556N, 115.878504E	eastward	153.873
9	2 Mar 2001	00:15:00	70.8	103.4	22.150878N, 115.256033E	eastward	92.076
	2 Mar 2001	00:20:00	70.95	95.3	22.297106N, 115.273566E	eastward	85.250
	2 Mar 2001	00:42:00	67.1	64.2	22.936563N, 115.390361E	eastward	65.227
5	2 Mar 2001	01:30:00	33.2	125.3	19.847633N, 117.901660E	eastward	197.869
	2 Mar 2001	01:50:00	37.9	114.98	20.709425N, 117.740585E	eastward	163.107
	2 Mar 2001	02:10:00	41.4	103.1	21.537934N, 117.600983E	eastward	133.368
	2 Mar 2001	03:25:00	42.8	93.3	22.361080N, 117.514960E	eastward	116.571
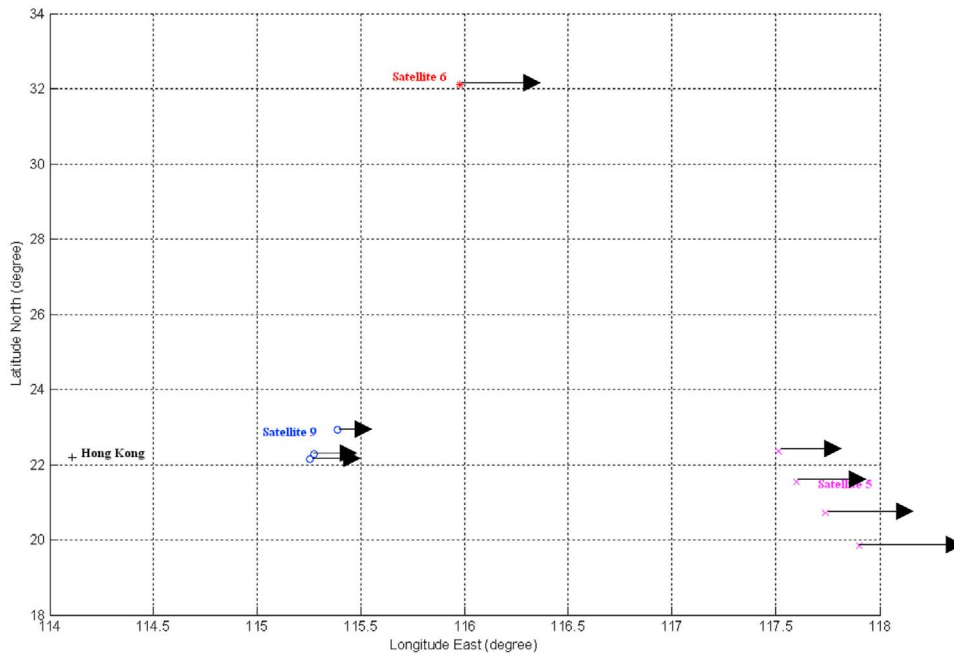
Figure 15. The map of IPP in Table 3 when scintillation velocity observed.

a midlatitude area and the other in Hong Kong, a low-latitude area.

[55] In California area, the estimated velocities are a little higher compared to previous research works with a general value around 100–200 m/s. The drift direction after midnight is westward, which is consistent with the previous research works.

[56] In the Hong Kong area, the velocity values are generally around 100–200 m/s, which is consistent with the previous research results. Different from that in California area, the estimated drift velocities are still in eastern direction after midnight, but their value is gradually decreasing over time.

[57] For our future work, to validate the estimated ionospheric drift velocities, experiments with close-spaced GPS receivers will be carried out and the results will be compared with that obtained with the proposed method in this research work.

[58] As the objective of this research work is proposing a method to monitor the equatorial ionospheric scintillation with local GPS network, not many research cases are provided. After the validity of the proposed method is confirmed, as the Hong Kong GPS reference network has been operating for many years, the proposed method will be used to investigate the scintillation in these years. We hope that the future research will tell us more about the equatorial ionospheric scintillation.

References

Aarons, J. (1977), Equatorials scintillations: A review, *IEEE Trans. Antennas Propag.*, 25, 729–736, doi:10.1109/TAP.1977.1141649.

Aarons, J. (1982), Global morphology of ionospheric scintillations, *Proc. IEEE*, 70, 360–378, doi:10.1109/PROC.1982.12314.

Aarons, J. (1993), The longitudinal morphology of equatorial F-layer irregularities relevant to their occurrence, *Space Sci. Rev.*, 63, 209–243, doi:10.1007/BF00750769.

Aarons, J., M. Mendillo, and R. Yantosca (1996), GPS phase fluctuations in the equatorial region, paper presented at 1996 Ionospheric Effects Symposium, Dep. of Defense, Alexandria, Va.

Abalde, J., P. Fagundes, Y. Sahai, and V. Pillat (2004), Height-resolved ionospheric drifts at low latitudes from simultaneous OI 777.4 nm and OI 630.0 nm imaging observations, *J. Geophys. Res.*, 109, A11308, doi:10.1029/2004JA010560.

Abdu, M., I. Kantor, I. Batista, and E. de Paula (1985), East-west plasma bubble irregularity motion determined from spaced VHF polarimeters: Implications on velocity shear in the zonal F region bulk plasma motion, *Radio Sci.*, 20(1), 111–122, doi:10.1029/RS020i001p00111.

Abdu, M., J. Sobral, Y. Nakamura, and C. Zamlutti (1987), Equatorial plasma bubble zonal velocity height gradient from spaced VHF polarimeter and scanning 630 nm measurements, *J. Geophys. Res.*, 14, 965–968.

Abdu, M., G. Walker, B. Reddy, J. Sobral, B. Fejer, T. Kikuchi, N. Trivedi, and E. Szuszczewicz (1990), Electrical field versus neutral wind control of the equatorial anomaly under quiet and disturbed condition — A global perspective, *Ann. Geophys.*, 8, 419–430.

Abdu, M., C. Denardini, J. Sobral, I. Batista, P. Muralikrishna, and E. de Paula (2002), Equatorial electrojet irregularities investigations using a 50MHz back-scatter radar and a digisonde at São Luís: Some initial results, *J. Atmos. Sol. Terr. Phys.*, 64, 1425–1434, doi:10.1016/S1364-6826(02)00106-2.

Abdu, M., I. Batista, H. Takahashi, J. MacDougall, J. Sobral, A. Medeiros, and B. Trivedi (2003), Magnetospheric disturbance induced equatorial plasma bubble development and dynamics: A case study in Brazilian sector, *J. Geophys. Res.*, 108(A12), 1449, doi:10.1029/2002JA009721.

Aggson, T., N. Maynard, F. Herrero, H. Mayr, L. Brace, and M. Liebrecht (1987), Geomagnetic equatorial anomaly in zonal plasma-flow, *J. Geophys. Res.*, 92, 311–315, doi:10.1029/JA092iA01p00311.

Anderson, D. (1973), A theoretical study of the ionospheric F region equatorial anomaly–I. Theory, *Planet. Space Sci.*, 21, 409–419, doi:10.1016/0032-0633(73)90040-8.

Argo, P., and M. Kelley (1986), Digital ionosonde observations during equatorial spread F, *J. Geophys. Res.*, 91, 5539–5555, doi:10.1029/JA091iA05p05539.

Banola, S., B. Pathan, D. Rao, and H. Chandra (2005), Spectral characteristics of scintillations producing ionospheric irregularities in the Indian region, *Earth Planets Space*, 57, 47–59.

Basu, S., et al. (1996), Scintillations, plasma drifts, and neutral winds in the equatorial ionosphere after sunset, *J. Geophys. Res.*, 101, 26,795–26,809, doi:10.1029/96JA00760.

Batista, I. S., E. R. de Paula, M. A. Abdu, N. B. Trivedi, and M. E. Greenspan (1991), Ionospheric effects of the March 13, 1989 magnetic storm at low and equatorial latitudes, *J. Geophys. Res.*, 96, 13,943–13,952, doi:10.1029/91JA01263.

Beach, T. L., and P. M. Kintner (1999), Simultaneous global positioning system observations of equatorial scintillations and total electron content fluctuations, *J. Geophys. Res.*, 104, 22,553–22,565, doi:10.1029/1999JA900220.

Beach, T., M. Kelley, P. Kintner, and C. Miller (1997), Total electron content variations due to nonclassical traveling ionospheric disturbances: Theory and global positioning system observations, *J. Geophys. Res.*, 102, 7279–7292, doi:10.1029/96JA02542.

Bhattacharyya, A., S. Basu, K. Groves, C. Valladares, and R. Sheehan (2002), Effect of magnetic activity on the dynamics of equatorial F region irregularities, *J. Geophys. Res.*, 107(A12), 1489, doi:10.1029/2002JA009644.

Blanc, M., and A. D. Richmond (1980), The ionospheric disturbance dynamo, *J. Geophys. Res.*, 85, 1669–1686, doi:10.1029/JA085iA04p01669.

Briggs, B. (1968), On the analysis of moving pattern in geophysics–I. Correlation analysis, *J. Atmos. Terr. Phys.*, 30, 1777–1788, doi:10.1016/0021-9169(68)90097-4.

Chen, W., S. Gao, C. Hu, Y. Chen, and X. Ding (2008), Effects of ionospheric disturbances on GPS observation in low latitude area, *GPS Solut.*, 12(1), 33–41, doi:10.1007/s10291-007-0062-z.

Coley, W., and R. Heelis (1989), Low-latitude zonal and vertical ion drifts seen by DE 2, *J. Geophys. Res.*, 94, 6751–6761, doi:10.1029/JA094iA06p06751.

Costa, E., and P. Fougere (1988), Cross-spectral analysis of spaced receiver measurement, *Radio Sci.*, 23(2), 129–139, doi:10.1029/RS023i002p00129.

Crain, D., R. Hellis, G. Bailey, and A. Richmond (1993), Low-latitude plasma drifts from a simulation of the global atmospheric dynamo, *J. Geophys. Res.*, 98, 6039–6046, doi:10.1029/92JA02196.

DasGupta, A., S. Basu, J. Aarons, J. Klobuchar, S. Basu, and A. Bushby (1983), VHF amplitude scintillations and associated electron content depletions as observed at Arequipa, Peru, *J. Atmos. Terr. Phys.*, 45, 15–26, doi:10.1016/S0021-9169(83)80003-8.

de Paula, E., et al. (2002), Ionospheric irregularity zonal velocities over Cachoeira Paulista, *J. Atmos. Sol. Terr. Phys.*, 64, 1511–1516, doi:10.1016/S1364-6826(02)00088-3.

de Paula, E., K. Iyer, D. Hysell, F. Rodrigues, F. S. Rodrigues, E. Kherani, A. Jardim, L. Rezende, S. Dutra, and N. Trivedi (2004), Multi-technique investigations of storm-time ionospheric irregularities over the São Luís equatorial station in Brazil, *Ann. Geophys.*, 22, 3513–3522, doi:10.5194/angeo-22-3513-2004.

Fagundes, P., Y. Sahai, I. Batista, J. Bitterncourt, M. Abdu, and H. Takashi (1997), Vertical and zonal equatorial *F* region plasma bubble velocities determined from OI 630 nm nightglow imaging, *Adv. Space Res.*, 20(6), 1297–1300, doi:10.1016/S0273-1177(97)00790-4.

Farges, T., and E. Blanc (2002), HF radar observations of irregularities in the daytime equatorial F region, *J. Atmos. Sol. Terr. Phys.*, 64, 1565–1571, doi:10.1016/S1364-6826(02)00094-9.

Farley, D., E. Bonelli, B. Fejer, and M. Larsen (1986), The prereversal enhancement of the zonal electric field in the equatorial ionosphere, *J. Geophys. Res.*, 91, 13,723–13,728, doi:10.1029/JA091iA12p13723.

Fejer, B. (1981), The equatorial ionospheric electric field: A review, *J. Atmos. Terr. Phys.*, 43, 377–386, doi:10.1016/0021-9169(81)90101-X.

Fejer, B. G. (1986), *Equatorial Ionospheric Electric Fields Associated With Magnetospheric Disturbances: Solar Wind-Magnetosphere Coupling*, Terra Sci., Tokyo.

Fejer, B. G., and L. Scherliess (1995), Time dependent response of equatorial ionospheric electric fields to magnetospheric disturbances, *Geophys. Res. Lett.*, 22, 851–854, doi:10.1029/95GL00390.

Fejer, B. G., R. A. Wolf, R. W. Spiro, and J. C. Foster (1990), Latitudinal variation of perturbation electric fields during geomagnetically disturbed periods: 1986 SUNDIAL observations and model results, *Ann. Geophys.*, *8*, 441–454.

Fejer, B., E. de Paula, S. Gonzalez, and R. Woodman (1991), Average vertical and zonal *F* region plasma drifts over Jicamarca, *J. Geophys. Res.*, *96*, 13,901–13,906, doi:10.1029/91JA01171.

Fejer, B., R. Heelis, and W. Hanson (1995), Global equatorial ionospheric vertical plasma drifts measured by the AE-E satellite, *J. Geophys. Res.*, *100*, 5769–5776, doi:10.1029/94JA03240.

Flaherty, J. P., M. C. Kelley, C. E. Seyler, and T. J. Fitzgerald (1996), Simultaneous VHF and transequatorial HF observations in the presence of bottomside equatorial spread F, *J. Geophys. Res.*, *101*, 26,811–26,818, doi:10.1029/96JA01115.

Hari Kishore, M., and G. Mukherjee (2007), Equatorial *F* region plasma drifts: A study using OI 630 nm emission all-sky images, *Curr. Sci.*, *93*(4), 488–496.

Heelis, R., P. Kendall, R. Moffett, D. Windle, and E. H. Rishbeth (1974), Electrical coupling of the E and F regions and its effect on F region drifts and winds, *Planet. Space Sci.*, *22*, 743–756, doi:10.1016/0032-0633(74)90144-5.

Hysell, D., and J. Burcham (1998), JULIA radar studies of equatorial spread F, *J. Geophys. Res.*, *103*, 29,155–29,167, doi:10.1029/98JA02655.

Hysell, D. L., M. F. Larsen, C. M. Swenson, A. Barjatya, T. F. Wheeler, M. F. Sarango, R. F. Woodman, and J. L. Chau (2005), Onset conditions for equatorial spread F determined during EQUIS II, *Geophys. Res. Lett.*, *32*, L24104, doi:10.1029/2005GL024743.

Immel, T., H. Frey, S. Mende, and E. Sagawa (2004), Global observations of the zonal drift speed of equatorial ionospheric plasma bubbles, *Ann. Geophys.*, *22*, 3099–3107, doi:10.5194/angeo-22-3099-2004.

Kelley, M. (1989), *The Earth's Ionosphere*, Academic, San Diego.

Kelley, M., D. Kotsikopoulos, T. Beach, D. Hysell, and S. Musman (1996), Simultaneous Global Positioning System and radar observations of equatorial spread F at Kwajalein, *J. Geophys. Res.*, *101*, 2333–2341, doi:10.1029/95JA02025.

Kikuchi, T., and T. Araki (1979), Horizontal transmission of the polar electric field to the equator, *J. Atmos. Terr. Phys.*, *41*, 927–936, doi:10.1016/0021-9169(79)90094-1.

Kil, H., P. Kintner, E. de Paula, and E. Kantor (2000), Global positioning system measurements of the ionospheric zonal apparent velocity at Cachoeira Paulista in Brazil, *J. Geophys. Res.*, *105*, 5317–5327, doi:10.1029/1999JA000244.

Kil, H., P. Kintner, E. de Paula, and I. Kantor (2002), Latitudinal variations of scintillation activity and zonal plasma drifts in South America, *Radio Sci.*, *37*(1), 1006, doi:10.1029/2001RS002468.

Kintner, P., and B. Ledvina (2004), Size, shape, orientation, speed, and duration of GPS equatorial anomaly scintillations, *Radio Sci.*, *39*, RS2012, doi:10.1029/2003RS002878.

Kintner, P., and B. Ledvina (2005), The ionosphere, radio navigation, and global navigation satellite systems, *Adv. Space Res.*, *35*(5), 788–811, doi:10.1016/j.asr.2004.12.076.

Kintner, P., H. Kil, T. Beach, and E. de Paula (2001), Fading timescales associated with GPS signals and potential consequences, *Radio Sci.*, *36*(4), 731–743, doi:10.1029/1999RS002310.

Klobuchar, J., D. Anderson, and P. Doherty (1991), Model studies of the latitudinal extent of the equatorial anomaly during equinoctial conditions, *Radio Sci.*, *26*(4), 1025–1047, doi:10.1029/91RS00799.

Makela, J., and M. Kelley (2003), Field-aligned 777.4 nm composite airglow images of equatorial plasma depletions, *Geophys. Res. Lett.*, *30*(8), 1442, doi:10.1029/2003GL017106.

Makela, J., B. Ledvina, M. Kelley, and P. Kintner (2004), Analysis of the seasonal variations of equatorial plasma bubble occurrence observed from Haleakala, Hawaii, *Ann. Geophys.*, *22*, 3109–3121, doi:10.5194/angeo-22-3109-2004.

Martinis, C., J. V. Eccles, J. Baumgardner, J. Manzano, and M. Mendillo (2003), Latitude dependence of zonal plasma drifts obtained from dual-site airglow observations, *J. Geophys. Res.*, *108*(A3), 1129, doi:10.1029/2002JA009462.

Mendillo, M., and J. Baumgardner (1982), Airglow characteristics of equatorial plasma depletions, *J. Geophys. Res.*, *87*, 7641–7652, doi:10.1029/JA087iA09p07641.

Mendillo, M., J. Baumgardner, X. Pi, P. Sultan, and R. Tsunoda (1992), Onset conditions for equatorial spread F, *J. Geophys. Res.*, *97*, 13,865–13,876, doi:10.1029/92JA00647.

Mendillo, M., J. Baumgardner, M. Colerico, and D. Nottingham (1997), Imaging science contributions to equatorial aeronomy: Initial results from the MISETA program, *J. Atmos. Terr. Phys.*, *59*, 1587–1599, doi:10.1016/S1364-6826(96)00158-7.

Mitra, S. (1949), A radio method of measuring winds in the ionosphere, *Proc. Inst. Electr. Eng.*, *96*, 441–446.

Moffett, R. (1979), The equatorial anomaly in the electron distribution of the terrestrial F region, *Fundam. Cosmic Phys.*, *4*, 313–391.

Mukherjee, G. (2003), Studies of the equatorial *F* region depletions and dynamics using multiple wavelength nightglow imaging, *J. Atmos. Sol. Terr. Phys.*, *65*, 379–390, doi:10.1016/S1364-6826(02)00214-6.

Musman, S., J. Jahn, J. LaBelle, and W. Swartz (1997), Imaging spread-F structures using GPS observations at Alcântara, Brazil, *Geophys. Res. Lett.*, *24*(13), 1703–1706, doi:10.1029/97GL00834.

Otsuka, Y., K. Shiokawa, and T. Ogawa (2002), Geomagnetic conjugate observations of equatorial airglow depletions, *Geophys. Res. Lett.*, *29*(15), 1753, doi:10.1029/2002GL015347.

Otsuka, Y., K. Shiokawa, and T. Ogawa (2006), Equatorial ionospheric scintillations and zonal irregularity drifts observed with closely spaced GPS receivers in Indonesia, *J. Meteorol. Soc. Jpn.*, *84A*, 343–351, doi:10.2151/jmsj.84A.343.

Paulson, M. (1984), Daytime equatorial scintillation of satellite signals at Guam, in *Effect of the Ionosphere on C3 I Systems*, edited by J. M. Goodman, pp. 179–185, U.S. Gov. Print. Off., Washington, D. C.

Pimenta, A., J. Bitterncourt, P. Fagundes, Y. Sahai, R. Buriti, H. Takahashi, and M. Taylor (2003a), Ionospheric plasma bubble zonal drifts over the tropical region: A study using OI 630nm emission all-sky images, *J. Atmos. Sol. Terr. Phys.*, *65*, 1117–1126, doi:10.1016/S1364-6826(03)00149-4.

Pimenta, A., P. Fagundes, Y. Sahai, J. Bittencourt, and J. Abalde (2003b), Equatorial *F* region plasma depletion drifts: Latitudinal and seasonal variations, *Ann. Geophys.*, *21*, 2315–2322, doi:10.5194/angeo-21-2315-2003.

Rama Rao, P., S. Tulasi Ram, D. Prasad, S. Gopi Krishna, and N. Lakshmi (2005), VHF and L-band scintillation characteristics over an Indian low latitude station, Waltair (17.7°N, 83.3°E), *Ann. Geophys.*, *23*, 2457–2464, doi:10.5194/angeo-23-2457-2005.

Richmond, A., S. Matsushita, and J. Tarpley (1976), On the production mechanism of electric currents and fields in the ionosphere, *J. Geophys. Res.*, *81*, 547–555, doi:10.1029/JA081i004p00547.

Rishbeth, H. (1971), Polarization fields produced by winds in the equatorial F region, *Planet. Space Sci.*, *19*, 357–369, doi:10.1016/0032-0633(71)90098-5.

Rohrbaugh, R., W. Hanson, B. Tinsley, B. Cragin, and J. McClure (1989), Images of transequatorial bubbles based on field-aligned airglow observations from Haleakela in 1984–1986, *J. Geophys. Res.*, *94*, 6763–6770, doi:10.1029/JA094iA06p06763.

Santana, D., J. Sobral, H. Takahashi, and M. Taylor (2001), Optical studies of the ionospheric irregularities over the Brazilian region by nocturnal images of the OI 630nm emission, *Adv. Space Res.*, *27*(6–7), 1207–1212, doi:10.1016/S0273-1177(01)00199-5.

Scherliess, L., and B. G. Fejer (1997), Strom time dependence of equatorial disturbance dynamo zonal electric field, *J. Geophys. Res.*, *102*, 24,037–24,046, doi:10.1029/97JA02165.

Sinha, H., and S. Raizada (2000), Some new features of ionospheric plasma depletions over the Indian zone using all sky optical imaging, *Earth Planets Space*, *52*, 549–559.

Sobral, J., and M. Abdu (1990), Latitudinal gradient in the plasma bubble zonal velocities as observed by scanning 630 nm airglow measurements, *J. Geophys. Res.*, *95*, 8253–8257, doi:10.1029/JA095iA06p08253.

Sobral, J., and M. Abdu (1991), Solar activity effects on equatorial plasma bubble zonal velocity and its latitude gradient as measured by airglow scanning photometers, *J. Atmos. Terr. Phys.*, *53*, 729–742, doi:10.1016/0021-9169(91)90124-P.

Spatz, D. E., S. J. Franke, and K. C. Yeh (1988), Analysis and interpretation of spaced receiver scintillation data recorded at an equatorial station, *Radio Sci.*, *23*(3), 347–361, doi:10.1029/RS023i003p00347.

Spiro, R. W., R. A. Wolf, and B. G. Fejer (1988), Penetration of highlatitude-electric-field effects to low latitudes during SUNDIAL 1984, *Ann. Geophys.*, *6*, 39–50.

Taylor, M., J. Eccles, J. LaBelle, and J. Sobral (1997), High resolution OI (630nm) image measurements of *F* region depletion drifts during the Guará Campaign, *Geophys. Res. Lett.*, *24*(13), 1699–1702, doi:10.1029/97GL01207.

Tinsley, B., P. Rohrbaugn, W. Hanson, and A. Broadfoot (1997), Images of transequatorial F region bubbles in 630- and 777-nm emissions compared with satellite measurements, *J. Geophys. Res.*, *102*, 2057–2077, doi:10.1029/95JA01398.

Tsunoda, R., and B. White (1981), On the generation and growth of equatorial backscatter plumes: 1. Wave structure in the bottomside F layer, *J. Geophys. Res.*, *86*, 3610–3616, doi:10.1029/JA086iA05p03610.

Valladares, C., R. Sheehan, S. Basu, H. Kuenzler, and J. Espinoza (1996), The multi-instrumented studies of equatorial thermosphere aeronomy

scintillation system: Climatology of zonal drifts, *J. Geophys. Res.*, *101*, 26,839–26,850, doi:10.1029/96JA00183.

Woodman, R. (1970), Vertical drift velocities and east-west electric fields at the magnetic equator, *J. Geophys. Res.*, *75*, 6249–6259, doi:10.1029/JA075i031p06249.

Woodman, R. (1972), East-west ionospheric drifts at the magnetic equator, *Space Res.*, *12*, 969–974.

Woodman, R., and C. La Hoz (1976), Radar observations of F region equatorial irregularities, *J. Geophys. Res.*, *81*, 5447–5466, doi:10.1029/JA081i031p05447.

Xu, J., J. Zhu, and L. Li (2007), Effects of a major storm on GPS amplitude scintillation phase fluctuations at Wuhan in China, *Adv. Space Res.*, *39*(8), 1318–1324, doi:10.1016/j.asr.2007.03.004.

W. Chen, X. Ding, and S. Ji, Department of Land Surveying and Geo-Informatics, Hong Kong Polytechnic University, Room HJ717, Hong Kong. (jidifferent@gmail.com)

C. Zhao, Chinese Academy of Surveying and Mapping, Beijing 100830, China.